Pressure-induced irreversible evolution of superconductivity in $PdBi_2$

Ying Zhou,[1,2] Xuliang Chen,[1] Chao An,[3] Yonghui Zhou,[1] Langsheng Ling,[1] Jiyong Yang,[1] Chunhua Chen,[1,2] Lili Zhang,[4] Mingliang Tian,[1,5] Zhitao Zhang,[1,*] and Zhaorong Yang[1,3,5,†]

[1]*Anhui Province Key Laboratory of Condensed Matter Physics at Extreme Conditions, High Magnetic Field Laboratory, Chinese Academy of Sciences, Hefei 230031, China*

[2]*University of Science and Technology of China, Hefei 230026, China*

[3]*Institute of Physical Science and Information Technology, Anhui University, Hefei 230601, China*

[4]*Shanghai Institute of Applied Physics, Chinese Academy of Sciences, Shanghai 201204, China*

[5]*Collaborative Innovation Center of Advanced Microstructures, Nanjing 210093, China*

(Received 13 October 2018; revised manuscript received 2 January 2019; published 4 February 2019)

Both α-$PdBi_2$ and β-$PdBi_2$ are superconductors with topological nontrivial signs. Here we report that the α-$PdBi_2$ superconductor is converted by pressure into the β-phase superconducting polymorph, with the superconductivity being further enhanced upon decompression. Through high-pressure resistance and synchrotron x-ray-diffraction experiments, we show that the α phase transforms into the β phase at $P_c \sim 8$ GPa, above which the superconductivity is robust up to the maximum pressure investigated in this work. More interestingly, when the applied pressure is gradually released from 42.9 down to 1.7 GPa, the T_c increases monotonously from 2.5 to 4.0 K. We argue that the observed unusual evolution of superconductivity can be explained by combination of pressure-manipulated crystal quality and the pressure dependence of T_c of the β-$PdBi_2$ superconductor.

DOI: 10.1103/PhysRevB.99.054501

I. INTRODUCTION

The $PdBi_2$ superconductors, including α-$PdBi_2$ and β-$PdBi_2$, have attracted much recent interest mainly because of the observations of topologically protected surface states, which makes them prospective candidates to realize topological superconductivity [1–17]. The β-$PdBi_2$ crystallizes in a layered tetragonal $CuZr_2$-type structure (*I4/mmm*) with superconducting transition T_c ranging from 4.25 to 5.4 K, depending on the quality of the crystal sample [1,2,14]. The mechanism of the superconductivity is still under hot debate so far, concerning multigap [2,3] or single-gap [4,7–9] nature of the superconductivity, and whether the topological surface state is important to superconductivity of the β-$PdBi_2$ [5,10,11] or not [7–9]. On the other hand, the α-$PdBi_2$ which forms a layered monoclinic ($C2/m$) structure is superconducting below 1.7 K [15–17]. More recently, Rashba surface states near Fermi level were theoretically predicted and experimentally identified via angle-resolved photoemission spectroscopy, suggesting that the Majorana fermion could be realized in the α-$PdBi_2$ by utilizing the Rashba states [15,16].

High pressure is a powerful method to investigate superconductivity, since it can effectively tune the lattice structure and electronic state [18,19]. Particularly, pressure is often used to explore for new superconductors from their nonsuperconducting parent compounds, such as the high-temperature superconductors [20,21], sulfur hydrides [22,23], and topological insulators [24,25]. For the $PdBi_2$ superconductors, to our knowledge, there were only two reports published about the pressure effect on the superconductivity in β-$PdBi_2$ and no relevant report on α-$PdBi_2$ [6,14]. It was reported that the T_c of the β-$PdBi_2$ decreases linearly with increasing pressure, but the highest measured pressure is limited to 2.4 GPa [6,14].

In this paper, we investigated the pressure effect on the superconductivity in α-$PdBi_2$. We found that the superconductivity is initially favored by pressure and then becomes almost pressure independent until a critical pressure of $P_c \sim 8$ GPa, where a structural transition from monoclinic α phase to tetragonal β phase is detected. Above P_c, the superconductivity in β-$PdBi_2$ is much more robust than expectation based on a linear extrapolation of the data below 2.4 GPa in previous reports [6,14]. Upon decompression from 42.9 GPa, the β phase is reserved to ambient condition but the T_c displays unusual irreversible pressure dependence.

II. METHODS

Single crystals of α-$PdBi_2$ were synthesized by flux method [17]. Stoichiometric mixture of Pd powder (99.999%) and Bi powder (99.999%) was sealed in an evacuated quartz tube. The tube was sintered at 900 °C for 24 h, then slowly cooled down to room temperature at a rate of 2–3 °C/h. The as-grown single crystals have distinct cleavage planes, with flat surfaces as large as $1 \times 1\,\mathrm{cm}^2$. The crystal structure and the stoichiometry of these single crystals were confirmed by single-crystal x-ray-diffraction (XRD) measurement (Cu $K\alpha$ radiation, $\lambda = 1.541\,84$ Å) and energy-dispersive x-ray spectrometry. Temperature-dependent resistivity of the α-$PdBi_2$ crystal was measured in different magnetic fields, using a standard four-point-probe method down to 0.5 K in a commercial ^{3}He refrigerator. Magnetization measurements were

*ztzhang@hmfl.ac.cn
†zryang@issp.ac.cn

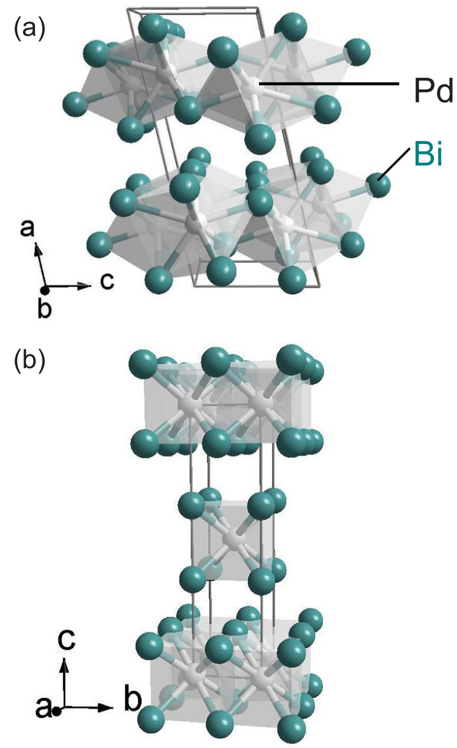

FIG. 1. (a) Schematic crystal structure of monoclinic α-$PdBi_2$, with space group of *C2/m*. (b) Schematic crystal structure of tetragonal β-$PdBi_2$, with space group of *I4/mmm*.

performed using a superconducting quantum interference device magnetometer.

High-pressure resistance measurements were performed in a nonmagnetic Be-Cu diamond-anvil cell. Diamond anvils of 300-μm culets and a T301 stainless-steel gasket covered with a mixture of epoxy and fine cubic boron nitride powder were used for high-pressure transport measurements. A single crystal with dimension of $100 \times 60 \times 10\,\mu\text{m}^3$ was loaded into the cell together with powdered NaCl powder as the pressure-transmitting medium. The cell was then put into an in-house multifunctional physical properties measurement system (T : $1.8 \sim 300\,\text{K}$; H : $0 \sim \pm 9\,\text{T}$). The resistance R was collected using the standard four-probe method via sweeping temperature.

High-pressure angle-dispersive synchrotron XRD experiments were performed with crushed $PdBi_2$ single crystals in a Mao-Bell cell at room temperature at the beamline BL15U1 of Shanghai Synchrotron Radiation Facility (SSRF). The x-ray wavelength is 0.6199 Å and neon gas was used as transmitting medium. The DIOPTAS [26] and RIETICA [27] programs were used for image integrations and XRD profile Rietveld refinements, respectively. Pressure was applied at room temperature and calibrated by using the ruby fluorescence shift for all experiments [28].

III. RESULTS AND DISCUSSION

In Fig. 1, we show the schematic crystal structures for α-$PdBi_2$ and β-$PdBi_2$, respectively, for the ease of understanding the results below. As one can see, the layers of monoclinic α-$PdBi_2$ are constructed with six-coordinated $PdBi_6$ building blocks, while tetragonal β-$PdBi_2$ consists of layers of eight-coordinated $PdBi_8$ building blocks. Noteworthy, the lattice volume *V/Z* (unit-cell volume per chemical

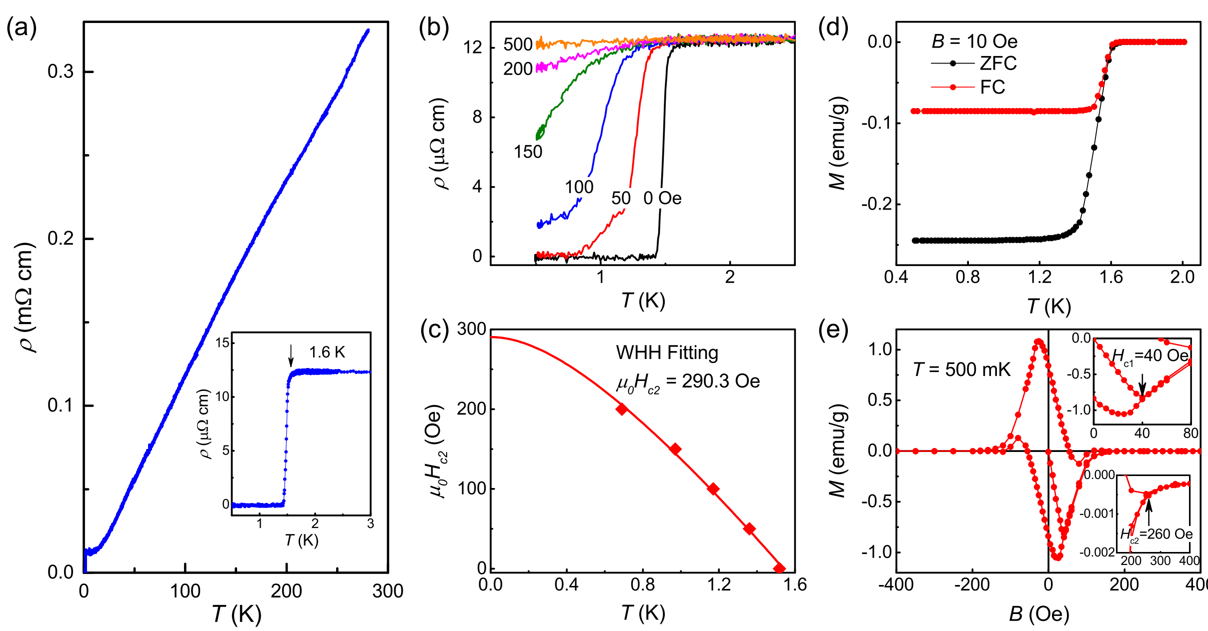

FIG. 2. (a) Temperature dependence of resistivity $\rho(T)$ for an α-$PdBi_2$ single-crystal sample. Inset: Zoom-in of the data near superconducting transition temperature. (b) $\rho(T)$ curves near superconducting transition measured in different magnetic fields up to 500 Oe, which is applied along the *a* axis. (c) Phase diagram of upper critical field $\mu_0 H_{c2}(T_c)$ versus temperature, where T_c was defined as the temperature with 90% of normal state resistivity. Closed diamonds represent the $\mu_0 H_{c2}(T)$ data. The solid lines represent the fitting line with the Werthamer-Helfand-Hohenberg model. (d) Magnetization of the α-$PdBi_2$ superconductor as a function of temperature with zero-field cooling (ZFC) and field-cooling (FC) sequences. (e) Magnetization of the α-$PdBi_2$ as a function of magnetic field at temperature of 0.5 K.

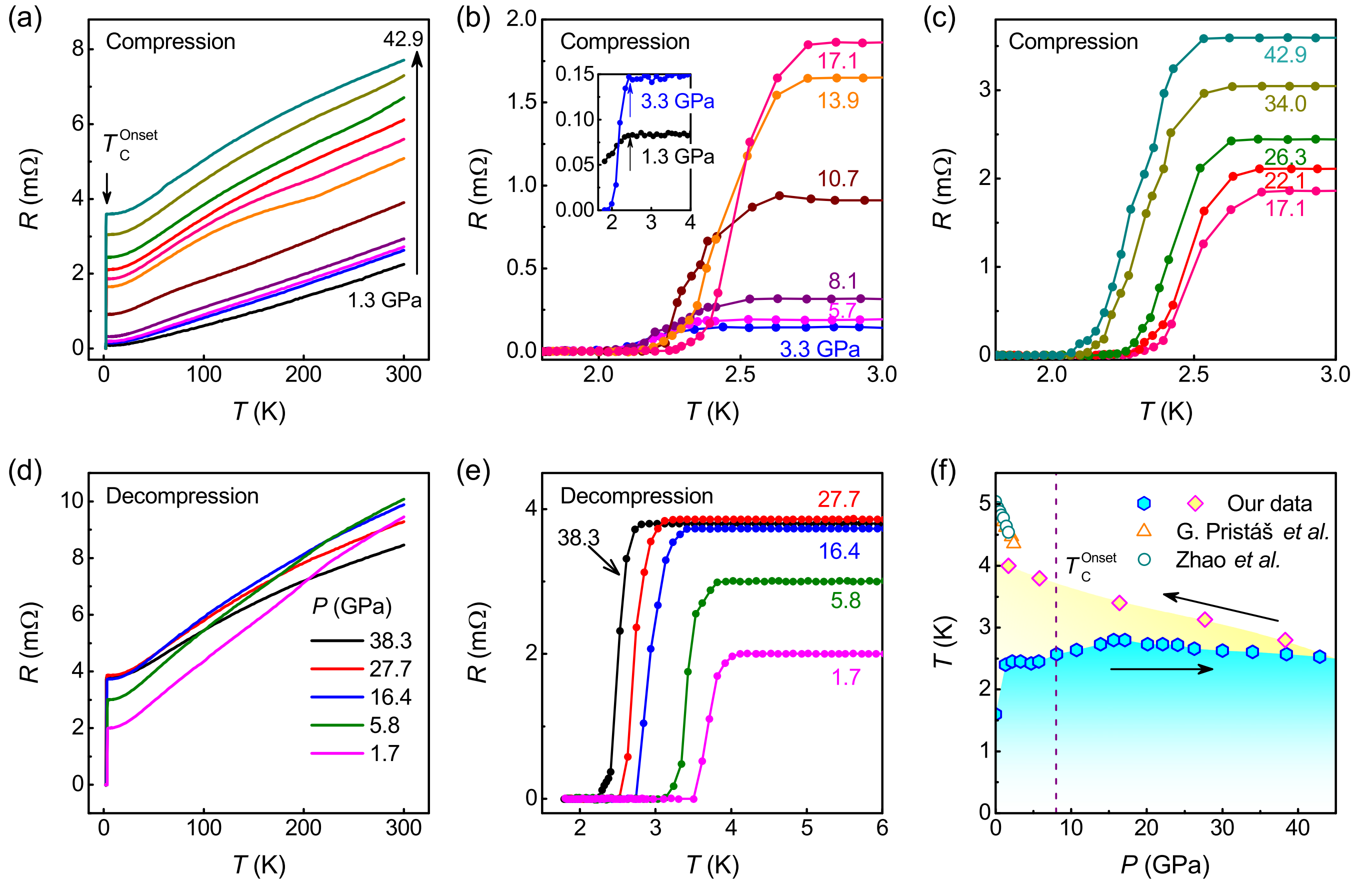

FIG. 3. (a) Temperature dependence of resistance $R(T)$ measured at different pressures in the compression process. (b), (c) Low-temperature zoom-ins of panel (a); the inset of (b) depicts the definition of T_c^{onset} by an arrow. (d) $R(T)$ curves in the decompression process. (e) Low-temperature zoom-in of panel (d). (f) Pressure-temperature phase diagram of the sample. The black arrows indicate the compression and decompression processes. For comparison, the pressure dependence of T_c for pure β-$PdBi_2$ from G. Pristáš *et al.* [14] and Zhao *et al.* [6] are also shown in the phase diagram.

formula) of α-$PdBi_2$, 75.58 Å^3, is slightly larger by ∼3% than the 73.38 Å^3 of β-$PdBi_2$.

Figure 2(a) displays the temperature dependence of resistivity $\rho(T)$ for an α-$PdBi_2$ single-crystal sample. As shown in the inset, a sharp superconducting resistive transition ($\Delta T_c \sim 0.17$ K) is observed at an onset transition temperature of $T_c^{\text{onset}} \sim 1.6$ K, which is close to the reported 1.7 K by other groups [16,17]. As for the normal state, the $\rho(T)$ shows a metallic behavior with a nearly linear temperature dependence in a large range from 300 down to 20 K, in agreement with previous reports [16,17]. The linear temperature dependence of resistivity was usually observed in unconventional superconductors, such as cuprates, iron pnictides, or heavy-fermion metals, and could be correlated with spin fluctuations near quantum criticality [29–31]. Here in the nonmagnetic compound α-$PdBi_2$, the origin of the linear behavior of resistivity is unclear. The value of residual resistivity ratio (27.1) is larger than that in previous reports [16,17], indicative of high quality of our sample.

Figure 2(b) displays the temperature dependence of resistivity for the α-$PdBi_2$ in different magnetic fields up to 500 Oe. Clearly, the superconducting transition was gradually suppressed with increasing magnetic field. In Fig. 2(c), we show the phase diagram of upper critical field $\mu_0 H_{c2}(T)$ against temperature. By fitting the data to the Werthamer-Helfand-Hohenberg (WHH) model [32], the zero-temperature upper critical field $\mu_0 H_{c2}(0)$ of 290 Oe is obtained. In Figs. 2(d) and 2(e), we show the results of magnetization measurements on an α-$PdBi_2$ single-crystal sample. As one can see from Fig. 2(d), the magnetization undergoes a sharp superconducting transition at 1.6 K, consistent with the resistivity measurements. Figure 2(e) evidences that the α-$PdBi_2$ superconductor is a type II superconductor, with the lower critical field of $\mu_0 H_{c1} = 40$ Oe nd the upper critical field of $\mu_0 H_{c2} = 260$ Oe, which is roughly equal to that obtained by WHH fitting of the resistivity data.

High-pressure resistance measurements up to 42.9 GPa were performed on an α-$PdBi_2$ single-crystal sample. In Figs. 3(a)–3(e), we show the recorded $R(T)$ curves at representative pressures both in compression and decompression processes, and summarize the T_c^{onset} versus pressure with a phase diagram in Fig. 3(f). As one can see in Fig. 3(a), the metallic conduction behavior in the normal state persists upon compression, with the entire $R(T)$ curve gradually upshifted. At the beginning pressure of 1.3 GPa, a small drop of resistance is observed at ∼2.4 K as seen from the inset of Fig. 3(b), although the α-$PdBi_2$ at ambient pressure is

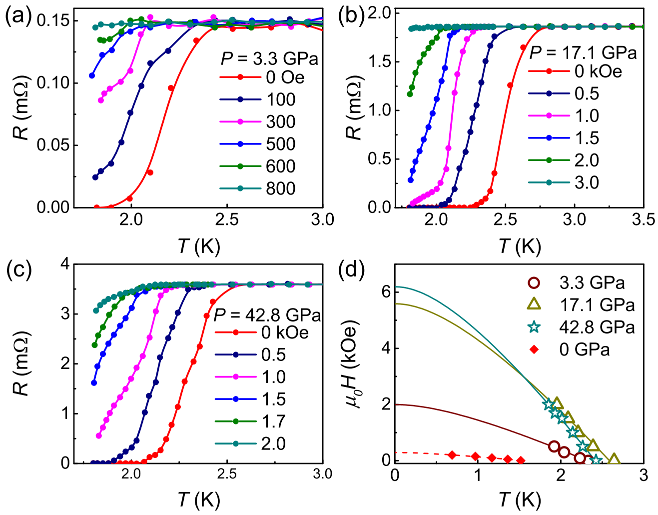

FIG. 4. Superconducting transition of the sample measured in magnetic fields $H \perp bc$ plane for pressures of (a) 3.3 GPa, (b) 17.1 GPa, and (c) 42.8 GPa. (d) Phase diagram of upper critical field $H_{c2}(T)$ versus temperature for the different pressures. The solid lines represent the fitting lines based on the WHH model. Here, T_c in the phase diagram was defined as the temperature with 90% of normal state resistance.

superconducting below 1.6 K. With further increasing pressure, the drop of resistance becomes more and more pronounced, which indicates that the superconductivity is favored under pressure. Zero resistance appears at 3.3 GPa and T_c^{onset} is almost pressure independent below a critical pressure point of $P_c \sim 8.1$ GPa. Above P_c, T_c^{onset} starts to increase until approaching a maximum of 2.8 K at 17.1 GPa and then gradually gets suppressed by pressure. In the decompression process, the metallic conduction behavior is not much changed, but unlike in the compression, the evolution of the $R(T)$ curve against pressure is not monotonous anymore. More surprisingly, the T_c^{onset} increases progressively up to 4.0 K with releasing pressure down to 1.7 GPa, rather than showing a reversible behavior; see Figs. 3(e) and 3(f).

In order to trace the pressure evolution of the upper critical field $\mu_0 H_{c2}(T)$, we measured the $R(T)$ curve under different magnetic fields at selected pressures of 3.3, 17.1, and 42.8 GPa. We present the recorded $R(T)$ curves in Figs. 4(a)–4(c) and show the summary of upper critical-field values in Fig. 4(d), together with the data for ambient pressure. At all pressures, the superconductivity is gradually suppressed with increasing magnetic field. Based on the WHH model fitting, the obtained $\mu_0 H_{c2}(0)$ are 2.0 kOe for 3.3 GPa, 6.2 kOe for 17.1 GPa, and 5.6 kOe for 42.8 GPa, respectively, which are dramatically enhanced compared with the 290.3 Oe at ambient pressure [see the red dashed line in Fig. 4(d)]. All the values are much lower than the Pauli limiting field of $H_P(0) = 1.84 T_c$ [33,34], suggesting that the dominant pair-breaking mechanism is not of Pauli type.

Motivated by the abnormally irreversible pressure dependence of T_c, we investigated the evolution of the lattice structure by performing angle-dispersive synchrotron XRD experiments on ground crystals of α-$PdBi_2$ under pressures up to 40.4 GPa. Representative XRD patterns are displayed in Fig. 5(a) and typical standard Rietveld refinements at 2.3 and 40.4 GPa are displayed in Fig. 5(b). Starting at 2.3 GPa,

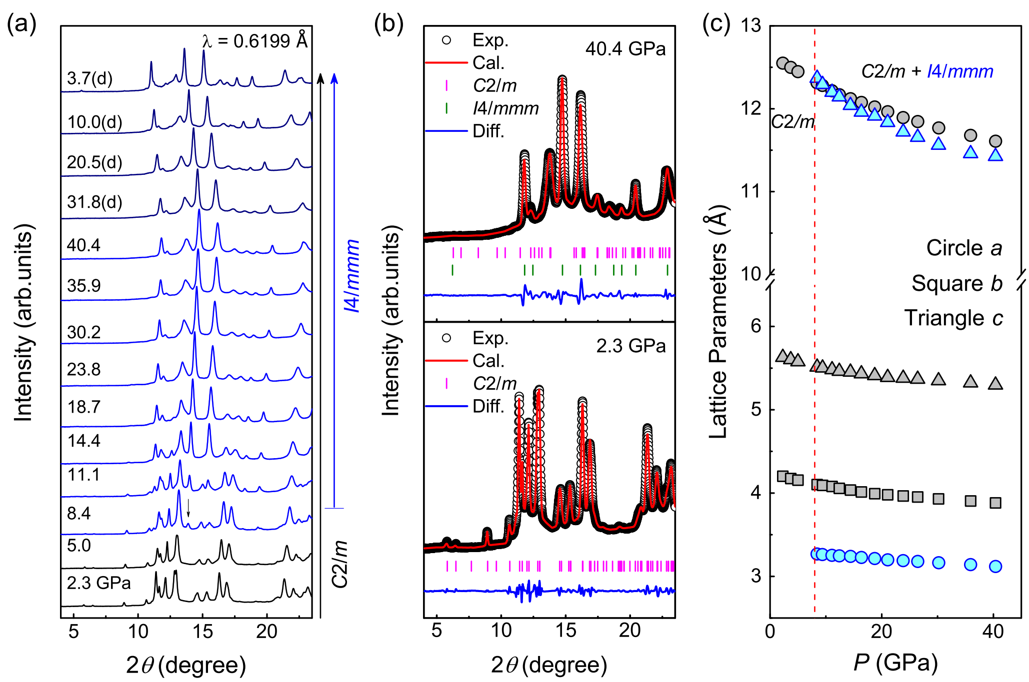

FIG. 5. (a) Typical high-pressure XRD patterns of the sample measured with pressure increasing from 2.3 to 40.4 GPa, and then decreasing to 3.7 GPa (labeled as "d"). A peak at 8.4 GPa indicated by arrow evidences a structural transition. (b) Representative Rietveld refinements of the XRD patterns at 2.3 and 40.4 GPa. (c) Pressure dependence of the refined lattice parameters a (circles), b (squares), and c (triangle) for the α-$PdBi_2$, as well as the high-pressure phase.

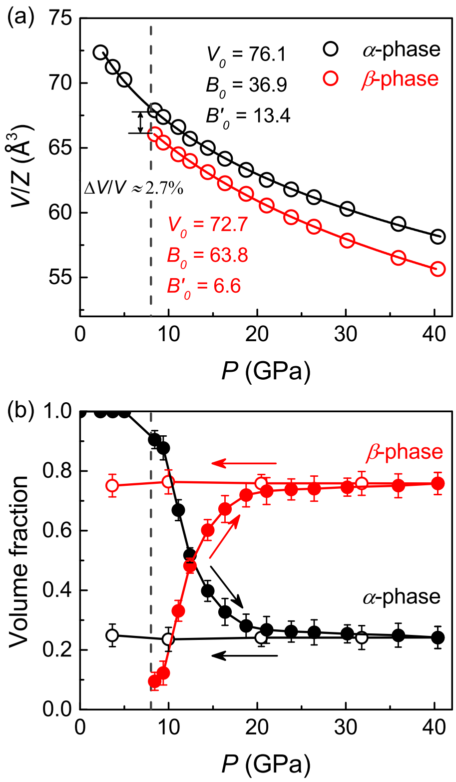

FIG. 6. (a) Unit-cell volume for both the α phase and high-pressure β phase of $PdBi_2$ as functions of pressure. The solid lines depict a fit to the experimental data using the third-order Birch-Murnaghan EOS [35]. (b) Pressure dependence of the volume fractions of α phase (black) and β phase (red).

the XRD pattern can be well indexed by single-phase monoclinic crystal structure with space group *C2/m* (No. 12), which is the same as that of α-$PdBi_2$ measured at ambient pressure. At 8.4 GPa, additional diffraction peaks begin to occur [see the arrow in Fig. 5(a)]. Two-phase Rietveld refinements of the XRD patterns above 8.4 GPa prove that the emergent high-pressure phase is in a tetragonal structure with space group *I*4/*mmm* (No. 144), which is the same as that of β-$PdBi_2$ at ambient pressure. It is found that the α phase and high-pressure β phase coexist until the highest measured pressure of 40.4 GPa. When the pressure is released down to 3.7 GPa (denoted by d), the XRD pattern is not much changed from the high-pressure one, except the shift in diffraction angles, indicative of the retention of the high-pressure structure. In Fig. 5(c), we present the gradual contraction of the lattice constants for both α- and β phases with increasing pressure.

The evolutions of volume *V/Z* (the unit-cell volume per chemical formula) with increasing pressure for the α phase and high-pressure β phase are plotted in Fig. 6(a). The isothermal equations of state (EoS) were fitted to the third-order Birch-Murnaghan formula [35]:

$$P = \tfrac{3}{2}B_0[(V_0/V)^{7/3} - (V_0/V)^{5/3}] \times \left\{1 + \tfrac{3}{4}(B'_0 - 4)[(V_0/V)^{2/3} - 1]\right\}, \qquad (1)$$

where V_0, B_0, and B'_0 are the zero-pressure volume, bulk modulus $-V/(dV/dP)$, and first-order derivative of the bulk modulus at zero pressure, respectively. The fitting yields $V_0 = 76.1\,\text{Å}^3$, $B_0 = 36.9$ GPa, and $B'_0 = 13.4$ for the α phase; and $72.7\,\text{Å}^3$, 63.8 GPa, and 6.6 for the high-pressure β phase. A volume collapse over the structural transition is detected and estimated to be $\Delta V/V \sim 2.7\%$, which characterizes a first-order transition. To provide a clear picture of the pressure-driven structural transition, we estimate the volume fractions of the two coexisting phases and present the results in Fig. 6(b). As one can see, the volume fraction of β phase begins to be detected at P_c and increases rapidly upon further compression. Beyond 17 GPa, the β-phase volume fraction gradually gets saturated and, simultaneously, the T_c changes to decay [see Fig. 3(f)].

At pressures below $P_c \sim 8$ GPa where the lattice structure of α-$PdBi_2$ is stable, the superconductivity is initially favored with T_c keeping a nearly constant value around 2.4 K. Similar pressure-independent feature of T_c was also observed in Bi_2Se_3, Cd_3As_2, and $PtBi_2$, which was considered as an indication of unconventional superconductivity [36–38]. Compared with α-$PdBi_2$, the β-$PdBi_2$ has a smaller unit-cell volume or a higher atomic density; therefore, the β phase would become more stable under high pressure. Above $P_c \sim 8$ GPa, the emergent β phase with a higher T_c coexists and competes with the original α phase, which leads to the increase of T_c. With further increasing pressure, while the growing volume fraction or improved sample quality of β phase contributes to an enhancement of T_c, the pressure itself may have a suppression effect on T_c of β phase. Actually, the pressure effect on the superconductivity of the β phase has been investigated by G. Pristáš *et al.* [14] and Zhao *et al.* [6]. Both reports show that the T_c decreases linearly with increasing pressure up to 2.4 GPa. If such linear correlation persists to higher pressures, the superconductivity would be completely suppressed at ~19.9 GPa. Nevertheless, we find that the superconductivity in the β phase is much more robust than expectation.

Interestingly, when the applied pressure is gradually released from 42.9 down to 1.7 GPa, the superconductivity gets enhanced monotonically. At first glance, the superconductivity enhancement could be assigned to the negative correlation between T_c and pressure in the β-$PdBi_2$ which is retained to ambient pressure. However, since the β phase dominates at pressures above $P_c \sim 8$ GPa in both compression and decompression processes, normally the evolution of T_c in decompression should follow the trend in compression at least above 8 GPa. As mentioned above, the T_c of β-$PdBi_2$ at ambient condition varies from 4.25 to 5.4 K depending on the sample quality [1,2,14]. After experiencing a pressure circling, the improvement of sample quality (i.e., crystallinity of β phase) could be expected. Thereby, the irreversible evolutions of T_c, including the decompression-induced enhancement, can be explained by competition between the pressure-manipulated sample quality and pressure effects on superconductivity in this pressure-quenchable phase. We note that similar behavior of decompression-enhanced superconductivity was also observed in In_2Se_3 [39]. We speculate that the scenario of pressure-enhanced sample quality might also apply to the situation in In_2Se_3, although a phonon softening mechanism is proposed there [39]. Further relevant researches are expected to address this issue.

IV. CONCLUSION

In summary, we have investigated the pressure effects on the superconductivity and structural properties of α-$PdBi_2$ single crystal. The α-$PdBi_2$ is stable up to $P_c \sim 8$ GPa, at which the structural transition to β-$PdBi_2$ was detected. Beyond P_c, a dome shape of T_c, as well as a pressure-quenchable or even a decompression-enhanced superconductivity, is observed and considered as a result of the competition between the improvement of sample quality and suppression effect of pressure on superconductivity in the β phase.

ACKNOWLEDGMENTS

This work was supported by the National Key Research and Development Program of China (Grants No. 2018YFA0305700 and No. 2016YFA0401804), the National Natural Science Foundation of China (Grants No. 11574323, No. U1632275, No. 11874362, No. U1832209, No. 11704387, No. 11804344, and No. 11605276), the Major Program of Development Foundation of Hefei Center for Physical Science and Technology (Grant No. 2018ZYFX002), the Users with Excellence Project of Hefei Science Center CAS (Grant No. 2018HSC-UE012), the Natural Science Foundation of Anhui Province (Grants No. 1808085MA06 and No. 1708085QA19). The x-ray diffraction experiment was performed at the beamline BL15U1, SSRF. We thank H. Y. Shu for his help with the HPSTAR equipment.

[1] B. T. Matthias, T. H. Geballe, and V. B. Compton, Rev. Mod. Phys. **35**, 1 (1963).
[2] Y. Imai, F. Nabeshima, T. Yoshinaka, K. Miyatani, R. Kondo, S. Komiya, I. Tsukada, and A. Maeda, J. Phys. Soc. Jpn. **81**, 113708 (2012).
[3] I. R. Shein and A. L. Ivanovskii, J. Supercond. Novel Magn. **26**, 1 (2013).
[4] E. Herrera, I. Guillamón, J. A. Galvis, A. Correa, A. Fente, R. F. Luccas, F. J. Mompean, M. García-Hernández, S. Vieira, J. P. Brison, and H. Suderow, Phys. Rev. B **92**, 054507 (2015).
[5] M. Sakano, K. Okawa, M. Kanou, H. Sanjo, T. Okuda, T. Sasagawa, and K. Ishizaka, Nat. Commun. **6**, 8595 (2015).
[6] K. Zhao, B. Lv, Y.-Y. Xue, X.-Y. Zhu, L. Z. Deng, Z. Wu, and C. W. Chu, Phys. Rev. B **92**, 174404 (2015).
[7] P. K. Biswas, D. G. Mazzone, R. Sibille, E. Pomjakushina, K. Conder, H. Luetkens, C. Baines, J. L. Gavilano, M. Kenzelmann, A. Amato, and E. Morenzoni, Phys. Rev. B **93**, 220504(R) (2016).
[8] L. Q. Che, T. Le, C. Q. Xu, X. Z. Xing, Z. X. Shi, X. F. Xu, and X. Lu, Phys. Rev. B **94**, 024519 (2016).
[9] J. Kačmarčík, Z. Pribulová, T. Samuely, P. Szabó, V. Cambel, J. Šoltýs, E. Herrera, H. Suderow, A. Correa-Orellana, D. Prabhakaran, and P. Samuely, Phys. Rev. B **93**, 144502 (2016).
[10] K. Iwaya, Y. Kohsaka, K. Okawa, T. Machida, M. S. Bahramy, T. Hanaguri, and T. Sasagawa, Nat. Commun. **8**, 976 (2017).
[11] Y. F. Lv, W. L. Wang, Y. M. Zhang, H. Ding, W. Li, L. L. Wang, K. He, C. L. Song, X. C. Ma, and Q. K. Xue, Sci. Bull. **62**, 852 (2017).
[12] H. Matsuzaki, K. Nagai, N. Kase, T. Nakano, and N. Takeda, J. Phys.: Conf. Ser. **871**, 012004 (2017).
[13] J.-J. Zheng and E. R. Margine, Phys. Rev. B **95**, 014512 (2017).
[14] G. Pristáš, M. Orendáč, S. Gabáni, J. Kačmarčík, E. Gažo, Z. Pribulová, A. Correa-Orellana, E. Herrera, H. Suderow, and P. Samuely, Phys. Rev. B **97**, 134505 (2018).
[15] H. Choi, M. Neupane, T. Sasagawa, E. E. M. Chia, and J.-X. Zhu, Phys. Rev. Mater. **1**, 034201 (2017).
[16] K. Dimitri, M. M. Hosen, G. Dhakal, H. Choi, F. Kabir, C. Sims, D. Kaczorowski, T. Durakiewicz, J.-X. Zhu, and M. Neupane, Phys. Rev. B **97**, 144514 (2018).
[17] S. Mitra, K. Okawa, S. Kunniniyil Sudheesh, T. Sasagawa, J.-X. Zhu, and E. E. M. Chia, Phys. Rev. B **95**, 134519 (2017).
[18] L. P. Gor'kov and V. Z. Kresin, Rev. Mod. Phys. **90**, 011001 (2018).
[19] H.-K. Mao, X.-J. Chen, Y. Ding, B. Li, and L. Wang, Rev. Mod. Phys. **90**, 015007 (2018).
[20] L. J. Zhang, Y. C. Wang, J. Lv, and Y. M. Ma, Nat. Rev. Mater. **2**, 17005 (2017).
[21] Q. Si, R. Yu, and E. Abrahams, Nat. Rev. Mater. **1**, 16017 (2016).
[22] A. P. Drozdov, M. I. Eremets, I. A. Troyan, V. Ksenofontov, and S. I. Shylin, Nature (London) **525**, 73 (2015).
[23] B. Keimer, S. A. Kivelson, M. R. Norman, S. Uchida, and J. Zaanen, Nature (London) **518**, 179 (2015).
[24] J. L. Zhang, S. J. Zhang, H. M. Weng, W. Zhang, L. X. Yang, Q. Q. Liu, S. M. Feng, X. C. Wang, R. C. Yu, L. Z. Cao, L. Wang, W. G. Yang, H. Z. Liu, W. Y. Zhao, S. C. Zhang, X. Dai, Z. Fang, and C. Q. Jin, Proc. Natl. Acad. Sci. USA **108**, 24 (2011).
[25] J. Zhu, J. L. Zhang, P. P. Kong, S. J. Zhang, X. H. Yu, J. L. Zhu, Q. Q. Liu, X. Li, R. C. Yu, R. Ahuja, W. G. Yang, G. Y. Shen, H. K. Mao, H. M. Weng, X. Dai, Z. Fang, Y. S. Zhao, and C. Q. Jin, Sci. Rep. **3**, 2016 (2013).
[26] C. Prescher and V. B. Prakapenka, High Pressure Res. **35**, 223 (2015).
[27] B. A. Hunter, RIETICA—A Visual Rietveld Program, International Union of Crystallography Commission on Powder Diffraction Newsletter No. 20 (Summer1998), http://www.rietica.org.
[28] H. K. Mao, J. Xu, and P. M. Bell, J. Geophys. Res. **91**, 4673 (1986).
[29] R. Daou, N. Doiron-Leyraud, D. LeBoeuf, S. Y. Li, F. Laliberté, O. Cyr-Choinière, Y. J. Jo, L. Balicas, J. Q. Yan, J. S. Zhou, J. B. Goodenough, and L. Taillefer, Nat. Phys. **5**, 31 (2008).
[30] H.v. Löhneysen, A. Rosch, M. Vojta, and P. Wölfle, Rev. Mod. Phys. **79**, 1015 (2007).
[31] S. Kasahara, T. Shibauchi, K. Hashimoto, K. Ikada, S. Tonegawa, R. Okazaki, H. Shishido, H. Ikeda, H. Takeya, K. Hirata, T. Terashima, and Y. Matsuda, Phys. Rev. B **81**, 184519 (2010).
[32] N. R. Werthamer, E. Helfand, and P. C. Hohenberg, Phys. Rev. **147**, 295 (1966).
[33] B. S. Chandrasekhar, Appl. Phys. Lett. **1**, 7 (1962).

[34] A. M. Clogston, Phys. Rev. Lett. **9**, 266 (1962).
[35] F. Birch, Phys. Rev. **71**, 809 (1947).
[36] K. Kirshenbaum, P. S. Syers, A. P. Hope, N. P. Butch, J. R. Jeffries, S. T. Weir, J. J. Hamlin, M. B. Maple, Y. K. Vohra, and J. Paglione, Phys. Rev. Lett. **111**, 087001 (2013).
[37] L. P. He, Y. T. Jia, S. J. Zhang, X. C. Hong, C. Q. Jin, and S. Y. Li, npj Quantum Mater. **1**, 16014 (2016).
[38] X. L. Chen, D. X. Shao, C. C. Gu, Y. H. Zhou, C. An, Y. Zhou, X. D. Zhu, T. Chen, M. L. Tian, J. Sun, and Z. R. Yang, Phys. Rev. Mater. **2**, 054203 (2018).
[39] F. Ke, H. N. Dong, Y. B. Chen, J. B. Zhang, C. L. Liu, J. K. Zhang, Y. Gan, Y. H. Han, Z. Q. Chen, C. X. Gao, J. S. Wen, W. G. Yang, X. J. Chen, V. V. Struzhkin, H. K. Mao, and B. Chen, Adv. Mater. **29**, 1701983 (2017).